

# Matrix-isolation FT-IR spectra and theoretical study of dimethyl sulfate

Ana Borba<sup>a</sup>, Andrea Gómez-Zavaglia<sup>a,b</sup>, Pedro N.N.L. Simões<sup>c</sup>, Rui Fausto<sup>a,\*</sup>

<sup>a</sup> Department of Chemistry, University of Coimbra, Coimbra P-3004-535, Portugal

<sup>b</sup> Facultad de Farmacia y Bioquímica, Universidad de Buenos Aires, Buenos Aires RA-1113, Argentina

<sup>c</sup> Department of Chemical Engineering, University of Coimbra, Coimbra P-3030-290, Portugal

Received 7 October 2004; accepted 29 October 2004

## Abstract

The preferred conformations of dimethyl sulfate and their vibrational spectra were studied by matrix-isolation FT-IR spectroscopy and theoretical methods (DFT and MP2, with basis sets of different sizes, including the quadruple-zeta, aug-cc-pVQZ basis). Conformer GG (of  $C_2$  symmetry and exhibiting O–S–O–C dihedral angles of  $74.3^\circ$ ) was found to be the most stable conformer in both the gaseous phase and isolated in argon. Upon annealing of the matrix, the less stable observed conformer (GT; with  $C_1$  symmetry) quickly converts to the GG conformer, with the resulting species being embedded in a matrix-cage which corresponds to the most stable matrix-site for GG form. The highest energy TT conformer, which was assumed to be the most stable conformer in previous studies, is predicted by the calculations to have a relative energy of ca.  $10 \text{ kJ mol}^{-1}$  and was not observed in the spectra of the matrix-isolated compound.

© 2004 Elsevier B.V. All rights reserved.

**Keywords:** FT-IR matrix-isolation spectroscopy; DFT and MP2 calculations; Dimethyl sulfate; Conformational and vibrational analysis

## 1. Introduction

Dimethyl sulfate ( $\text{DMSO}_4$ ) is an industrial chemical that is used as alkylating agent to convert compounds such as phenols, amines and thiols to the corresponding methyl derivatives, used in the industrial production of dyes, perfumes and polyurethane-based adhesives [1,2]. It is also used as intermediate in the manufacture of many pharmaceuticals (e.g., antipyretics and anticholinergics), pesticides and as solvent in the separation of mineral oils [3,4].  $\text{DMSO}_4$  has been shown to produce tumors in laboratory animals [5,6] and is also considered to be a human carcinogen [7]. Being extremely toxic, methods like gas chromatography and optical spectrometry have been applied for its determination in the environment [8,9]. However, in spite of the well known chemical and biochemical importance of  $\text{DMSO}_4$ , the available knowledge on its structural and vibrational properties is very scarce. To the best of our knowledge, no theoretical structural studies have been reported on this compound, while the most recent

infrared/Raman spectroscopic study on  $\text{DMSO}_4$  was published more than 30 years ago [9].

One of the main difficulties to study this compound (and in general the family of compounds with sulfur-to-oxygen linkages) by theoretical methods has been the relatively large computational resources required to undertake reliable predictions of their fundamental properties. On the other hand, the peculiarities of the sulfur-to-oxygen linkages are far from being well understood, and the most currently used methods of calculation have not yet been tested sufficiently when applied to this kind of systems. For example, it is well known that theoretical predictions of vibrational spectra of molecules with more usual linkages (e.g., CH, CO, CN, NO, NH, OH, etc.) by ab initio or density functional theory (DFT) based methods usually lead to a general systematic overestimation of the vibrational frequencies, thus enabling the uniform scaling procedure to be applied successfully in order to fit the calculated spectra to the experimental data. However, it was found that this is not the case for molecules with SO bonds, where the theory often yields frequencies that underestimate the experimentally observed ones. This behavior has been found even for molecules as simple as SSO

\* Corresponding author. Tel.: +351 239 827 703; fax: +351 239 852 080.  
E-mail address: [rfausto@ci.uc.pt](mailto:rfausto@ci.uc.pt) (R. Fausto).

[10]. Besides, it is also well known that the accumulated knowledge on the molecular structures, conformational and spectroscopic properties, and chemical reactivity in general, of sulfur compounds is still incipient when compared, for instance, with that of their oxygen analogue compounds.

The second important difficulty for studying sulfur (or mixed sulfur/oxygen) compounds is of practical nature: the compounds usually are relatively difficult to crystallize, decompose easily both upon heating and/or light exposition and, in many cases, as in  $\text{DMSO}_4$ , which was used in the First World War as war-gas [11], are highly toxic to human beings [12,13]. Then, besides its more fundamental interest, characterization of  $\text{DMSO}_4$  regarding its structural and spectroscopic properties is also important to improve the efficiency of its industrial manipulation and environmental control.

In this work,  $\text{DMSO}_4$  was studied by low temperature matrix-isolation FT-IR spectroscopy and computational methods [both density functional theory (DFT) and ab initio second-order Moller–Plesset (MP2) methods], in order to investigate its conformational preferences and spectroscopically characterize its conformationally dependent vibrational properties.

## 2. Materials and methods

### 2.1. Infrared spectroscopy

Dimethyl sulfate was obtained from Aldrich (purity 99%). The IR spectra were collected, with  $0.5\text{ cm}^{-1}$  spectral resolution, on a Mattson (Infinity 60AR Series) Fourier transform infrared spectrometer, equipped with a deuterated triglycine sulfate (DTGS) detector and Ge/KBr beamsplitter.

In the matrix-isolation experiments, a glass vacuum system and standard manometric procedures were used to deposit the matrix gas (argon N60, obtained from Air Liquide). Matrices were prepared by co-deposition, onto the cooled CsI substrate of the cryostat, of the matrix gas and  $\text{DMSO}_4$ , which was sublimated using a specially designed doubly thermostatable Knudsen cell with shut-off possibility [14]. The container of the Knudsen cell was kept at  $0^\circ\text{C}$  to reduce the vapor pressure of the compound over the solid and enable a better control of the amount of  $\text{DMSO}_4$  being deposited. Temperatures of the nozzle varied from room temperature to  $200^\circ\text{C}$ . All experiments were done on the basis of an APD Cryogenics close-cycle helium refrigeration system with a DE-202A expander. Deposition temperatures used range from 9 to 20 K. Necessary modifications of the sample compartment of the spectrometer were made in order to accommodate the cryostat head and allow efficient purging of the instrument by a stream of dry  $\text{N}_2$  to remove water and  $\text{CO}_2$  vapors. After depositing the compound, annealing experiments were performed until a temperature of 42 K.

### 2.2. Computational methodology

The quantum chemical calculations were performed with Gaussian '98 [15] at the DFT and MP2 levels of theory, using the 6-311++G(d,p), 6-31++G(d,p) and aug-cc-pVQZ basis sets [16–25]. The DFT calculations were carried out with the three-parameter density functional abbreviated as B3LYP, which includes Becke's gradient exchange correction [26] and the Lee, Yang and Parr correlation functional [27].

Conformations were optimized using the geometry direct inversion of the invariant subspace (GDIIS) method [28]. Vibrational frequencies were calculated at each level of theory and the nature of the stationary points on the potential energy surface (PES) resulting from optimization was determined by inspection of the corresponding calculated Hessian matrix. The optimized structures of all conformers described in this study were confirmed to correspond to true minimum energy conformations on the different potential energy surfaces investigated. Potential energy profiles for internal rotation were calculated performing a relaxed scan on the PES along the relevant reaction coordinates, and the transition state structures for conformational interconversion obtained using the synchronous transit-guided quasi-Newton (STQN) method [29].

Normal coordinate analyses were undertaken in the internal coordinates space as described by Schachtschneider [30], using the program BALGA and the optimized geometries and harmonic force constants resulting from the B3LYP/aug-cc-pVQZ calculations.

## 3. Results and discussion

### 3.1. Geometries and energies

$\text{DMSO}_4$  has four different internal rotation axes, defined around the S–O and O–C bonds, that can, in principle, give rise to conformational isomers. In order to search for minimum energy conformations, a systematic investigation of the potential energy surface of the molecule was undertaken using the B3LYP/6-311++G(d,p) method. All non-equivalent-by-symmetry possible combinations of the four dihedral angles corresponding to staggered structures were used as initial geometries in the optimization procedures, as well as those where at least one O–S–O–C dihedral was  $\pm 120^\circ$ . This corresponds to a subset of 50 unique structures from the whole set of 144 possible conformations defined by the selected dihedrals. In spite of the large number of trial structures, the calculations yield only three different energy minima, corresponding to two conformers with  $\text{C}_2$  symmetry and one form belonging to the  $\text{C}_1$  point group (see Fig. 1, where the naming adopted to designate each form is given). After reoptimization of these three structures at the B3LYP/aug-cc-pVQZ level of theory their characteristic C–O–S–O dihedral angles were found to be equal to  $(74.3^\circ, 74.3^\circ)$ ,  $(177.1^\circ, 177.1^\circ)$  and  $(73.5^\circ, -173.0^\circ)$ , respectively, for GG, TT and GT forms. In all cases the methyl groups assume the conformation

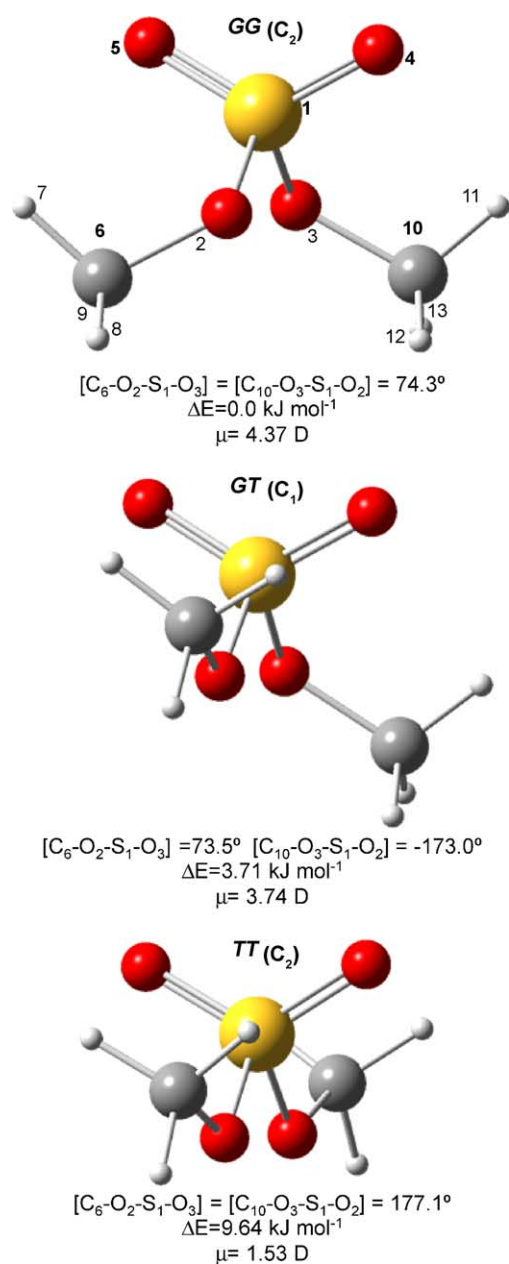


Fig. 1. Conformers of DMSO<sub>4</sub> with atom numbering scheme. Defining dihedral angles, relative energies and dipole moments are also shown.

where one of the CH bonds is anti-periplanar relatively to the S–O bond (the barrier for rotation of the methyl groups around the C–O bond was calculated as ca. 5 kJ mol<sup>-1</sup>). Table 1 presents the calculated relative energies of the three conformers at the different levels of calculation used in this study, as well as their populations at room temperature (298 K) and at other temperatures relevant in the context of this investigation (393, 423 and 463 K), estimated using the B3LYP/aug-cc-pVQZ relative energies and the Boltzman distribution. The optimized geometries are provided as Electronic Supplementary Material (ESI), Table S01.

The most stable conformer of DMSO<sub>4</sub> is form GG, which is similar to the most stable conformation of sulfuric acid [31]. The relative stability of the three conformers can be easily correlated with the number of repulsive interactions between the non-bonding pairs of electrons of the methoxylic oxygen atoms: in the most stable form (conformer GG) there are no such interactions, while the second most stable form (GT) and less stable form (TT) exhibit one and two oxygen lone-electron pair repulsive interactions, respectively. It is worth noting that the relative energy of the TT conformer is predicted at all levels of theory to be considerably larger than twice the relative energy of the GT form (at the B3LYP/aug-cc-pVQ level of theory, it is about three times greater; see Table 1), as expected taking into account that in GT the C–O–S–O dihedrals can significantly deviate from the sterically more relevant values (60°, 180°) to minimize the repulsive interactions. Indeed, as mentioned above, in GT these dihedral angles were found to be (73.5°, -173.0°). In TT, there is no such conformational flexibility, though a slightly distortion from planarity of the heavy-atom backbone was also predicted by the calculations, leading to the observed dihedral angles of (177.1°, 177.1°) and to definition of the symmetry of the conformer as C<sub>2</sub>, instead of C<sub>2v</sub> as for the planar configuration.

Another geometrical parameter that was found to reflect the importance of the repulsive interactions between the methoxyl oxygen lone electron pairs is the distance between the two methoxy oxygen atoms. This distance increases along the series TT, GT, GG (236.6, 242.2 and 251.7 pm, respectively), clearly indicating that once there is space available the two oxygen atoms tend to move away from each other. In conformers GT and TT, the position of one or of the two methyl groups near the S=O bonds, respectively, hinders the opening of the O–S–O angle and does not allow

Table 1  
Relative energies, including zero point vibrational contributions, for the various conformers of dimethyl sulfate<sup>a</sup>

Conformer	$\Delta E_{ZPE}$			Population <sup>b</sup> (%)			
	B3LYP/6-311++G(d,p)	MP2/6-31++G(d,p)	B3LYP/aug-cc-pVQZ	298 K	393 K	423 K	463 K
GG	0.0 (-2044920.73) <sup>c</sup>	0.0 (-2037407.38) <sup>c</sup>	0.0 (-2045265.051) <sup>c</sup>	68.2	59.0	56.8	54.2
GT	2.63	5.41	3.71	30.5	37.9	39.5	41.3
TT	9.99	13.59	9.64	1.4	3.1	3.7	4.4

<sup>a</sup> Energies in kJ mol<sup>-1</sup>; conformers are depicted in Fig. 1.

<sup>b</sup> Estimated using relative energies optimized at the B3LYP/aug-cc-pVQZ level of theory.

<sup>c</sup> Total energies with zero point vibrational energy contribution.

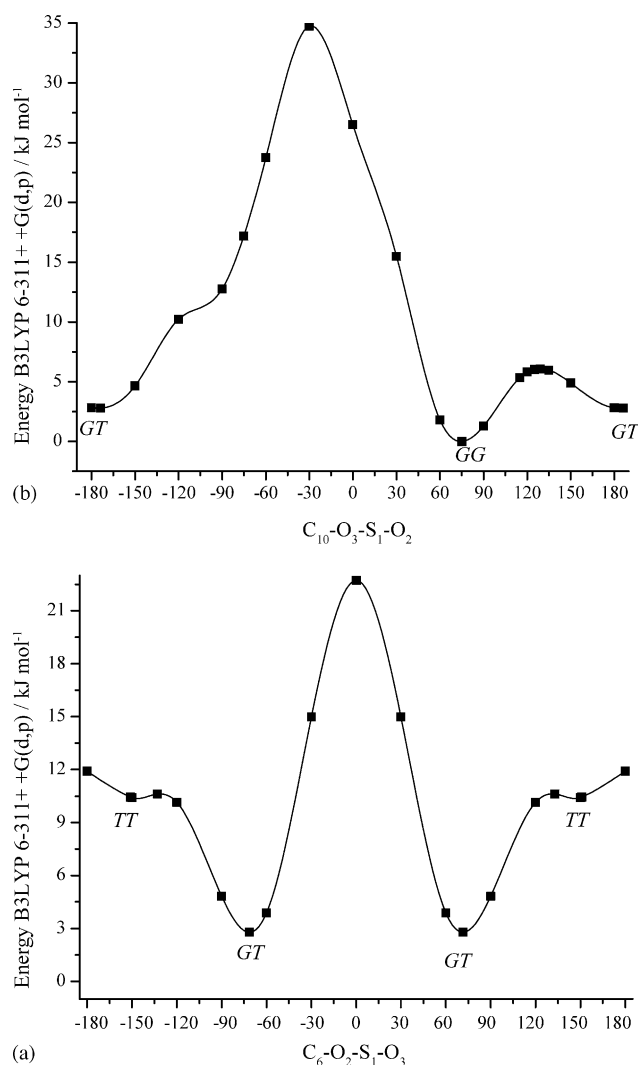


Fig. 2. B3LYP/6-311++G(d,p) calculated potential energy profiles for conformational interconversion: (a) GG  $\leftrightarrow$  GT; (b) TT  $\leftrightarrow$  GT.

the accompanying energy release (this effect is, naturally, larger in TT, since in this case no space for opening of the O–S–O angle is available in *both* sides of the molecule).

In general, the predictions made at the three levels of theory used are qualitatively identical. However, contrarily to the remaining methods, the B3LYP/aug-cc-pVQZ calculations predict the two geometry of the heavy atom skeleton of the third conformer close to planarity (C–O–S–O dihedrals angles equal to 177.1°, versus ca. 150–160° with B3LYP/6-311++G\*\* and MP2/6-311++G\*\*; see Table S01). The potential energy profiles leading to interconversion between the different conformers are shown in Fig. 2. The curves were obtained at the B3LYP/6-311++G\*\* level, since their computation at the B3LYP/aug-cc-pVQZ would require a non-affordable amount of computer time, while the main characteristics of the profiles calculated with the two basis should not differ substantially. As shown Fig. 2a, the highest energy conformer is surrounded by very low energy barriers: the B3LYP/6-311++G\*\* barrier separating this conformer

from its equivalent by symmetry form (corresponding to the planar  $C_{2v}$  transition state with C–O–S–O dihedral angles of 180°) is 0.68 kJ mol<sup>-1</sup>, while that leading to conversion to conformer GT is as low as 0.22 kJ mol<sup>-1</sup>. At the B3LYP/aug-cc-pVQZ level, the first energy barrier shall be lower and the last slightly higher than as calculated with the 6-311++G\*\* basis set, but both barriers are not expected to be much different from those presented in Fig. 2. Depending on the basis set used for calculation, the zero-point energies associated with the torsional modes corresponding to the reaction coordinates converting the highest energy conformer into its equivalent by symmetry form ( $\tau(S-O)$ s) or conformer GT ( $\tau(S-O)$ ) as) were predicted to be 0.08–0.33 and 0.23–0.31 kJ mol<sup>-1</sup>, respectively (see also Table S05; ESI). Hence, in both cases the zero-point energy is of the same order of magnitude of the energy barrier, in particular in the case of the channel leading to conversion of TT into GT, and the physical relevance of conformer TT is questionable. Indeed, this form should be better described as a higher vibrationally excited torsional state of conformer GT.

Fig. 2b presents the potential energy profile for GT  $\leftrightarrow$  GG interconversion. The profile is strongly asymmetric, with barriers associated with the two paths for conversion of form GT into GG equal to 31.9 and 3.29 kJ mol<sup>-1</sup>. The first is the longest reaction pathway, implying a rotation of ca. 280° around the C–O–S–O axis, and corresponds to the rotation of the C–O–S–O axis initially in the *trans* configuration in the direction which leads the two methyl groups to pass through the considerably strained face-to-face position. The second reaction path corresponds to the shortest rotation in the opposite direction and is practically unstrained, which justifies the low energy barrier. In the context of the present study, the low energy pathway for the GT  $\rightarrow$  GG conversion is particularly relevant. The predicted energy barrier for this conversion is large enough to allow initial trapping of the two conformers (GT and GG) in the low temperature inert matrices, but it is also small enough to be overcome by annealing of the matrices and enable conformational isomerization to take place.

In summary, the theoretical predictions reveal that both GG and GT forms can be expected to be observed in the as-deposited matrices, the GT conformer being convertible into the most stable GG form by annealing of the matrices to higher temperatures. The TT conformer is predicted not to be of any practical relevance, being better described as a highly excited state of the GT form. Assuming that GG is a doubly degenerated form and that the degree of conformational degenerescence of GT is 4, at room temperature (298 K) the predicted populations for the two conformers, taking into account the B3LYP/aug-cc-pVQZ calculated energies, are 68% for GG and 32% for GT; at 463 K (the highest temperature used for deposition of the matrices) these populations are 57% and 43%, respectively. Then, both forms are predicted to be present in the initially deposited matrices and the increase of the relative population of conformer GT with the temperature of deposition appears to be large enough to be observable experimentally. As described in detail in the

Table 2

Observed frequencies for the (a) GG<sup>a</sup> and (b) GT<sup>b</sup> forms of dimethyl sulfate monomer in argon matrix

Approximate description	Symmetry	Calculated frequency	Intensity	Observed Ar (9 K)
<b>(a) GG form</b>				
$\nu(\text{CH}_3)'_{\text{as}} \text{ s}$	A	3158.8	3.5	3047.4
$\nu(\text{CH}_3)'_{\text{as}} \text{ as}$	B	3158.8	5.8	
$\nu(\text{CH}_3)''_{\text{as}} \text{ s}$	A	3135.1	3.7	3026.3
$\nu(\text{CH}_3)''_{\text{as}} \text{ as}$	B	3134.5	17.9	3022.6
$\nu(\text{CH}_3)_{\text{s}} \text{ s}$	A	3053.9	24.1	2970.3
$\nu(\text{CH}_3)_{\text{s}} \text{ as}$	B	3053.3	28.5	<b>2968.0</b> , 2966.9
$\delta(\text{CH}_3)''_{\text{as}} \text{ s}$	A	1507.3	6.1	1469.2
$\delta(\text{CH}_3)''_{\text{as}} \text{ as}$	B	1503.8	19.3	1465.2
$\delta(\text{CH}_3)'_{\text{as}} \text{ as}$	B	1490.8	6.5	1454.7
$\delta(\text{CH}_3)'_{\text{as}} \text{ s}$	A	1490.1	7.1	
$\delta(\text{CH}_3)_{\text{s}} \text{ as}$	B	1474.1	4.7	1446.8
$\delta(\text{CH}_3)_{\text{s}} \text{ s}$	A	1470.7	1.5	1437.6
$\nu(\text{S}=\text{O}) \text{ as}$	B	1410.0	248.2	1417.6, <b>1415.5</b>
$\nu(\text{S}=\text{O}) \text{ s}$	A	1197.9	127.2	1216.0
$\gamma(\text{CH}_3)''_{\text{as}}$	B	1194.2	4.8	1211.8
$\gamma(\text{CH}_3)''_{\text{s}}$	A	1189.5	50.5	1210.4
$\gamma(\text{CH}_3)'_{\text{s}}$	A	1178.9	8.5	1179.3
$\gamma(\text{CH}_3)'_{\text{as}}$	B	1177.8	1.7	
$\nu(\text{C}-\text{O}) \text{ s}$	A	1022.4	138.6	<b>1025.1</b> , 1022.9
$\nu(\text{C}-\text{O}) \text{ as}$	B	1010.6	257.8	<b>1008.3</b> , 1006.2
$\nu(\text{S}-\text{O}) \text{ as}$	B	790.9	288.9	<b>821.9</b> , 819.9
$\nu(\text{S}-\text{O}) \text{ s}$	A	729.0	64.4	755.8
$\gamma(\text{SO}_2)$	B	586.0	12.2	<b>594.2</b> , 592.2, 576.0
$\delta(\text{O}=\text{S}=\text{O})$	A	549.6	23.0	<b>572.6</b> , <b>570.4</b>
$w(\text{SO}_2)$	B	490.0	21.7	<b>505.6</b> , 503.3
$\text{tw}(\text{SO}_2)$	A	413.0	9.6	426.6
Approximate description		Calculated frequency	Intensity	Observed Ar (9 K)
<b>(b) GT form</b>				
$\nu(\text{CH}_3)''_{\text{as}} \text{ as}$		3162.0	4.5	3047.4
$\nu(\text{CH}_3)''_{\text{as}} \text{ s}$		3155.6	5.7	
$\nu(\text{CH}_3)'_{\text{as}} \text{ as}$		3141.2	8.7	3026.3
$\nu(\text{CH}_3)'_{\text{as}} \text{ s}$		3128.0	8.4	3018.6
$\nu(\text{CH}_3)_{\text{s}} \text{ s}$		3058.1	25.8	2972.5
$\nu(\text{CH}_3)_{\text{s}} \text{ as}$		3049.7	29.3	2962.7
$\delta(\text{CH}_3)''_{\text{as}} \text{ s}$		1507.4	12.6	1469.2
$\delta(\text{CH}_3)''_{\text{as}} \text{ as}$		1505.5	11.7	
$\delta(\text{CH}_3)'_{\text{as}} \text{ s}$		1493.2	3.8	1457.6
$\delta(\text{CH}_3)'_{\text{as}} \text{ as}$		1490.7	6.9	1454.7
$\delta(\text{CH}_3)_{\text{s}} \text{ s}$		1473.1	0.8	1437.6
$\delta(\text{CH}_3)_{\text{s}} \text{ as}$		1470.5	1.3	
$\nu(\text{S}=\text{O}) \text{ as}$		1387.7	266.0	1397.5
$\gamma(\text{CH}_3)''_{\text{as}}$		1200.4	71.1	1216.0
$\gamma(\text{CH}_3)''_{\text{s}}$		1195.7	15.1	1211.8
$\nu(\text{S}=\text{O}) \text{ s}$		1185.4	94.8	1206.7, 1205.0
$\gamma(\text{CH}_3)'_{\text{as}}$		1177.4	1.6	1178.6
$\gamma(\text{CH}_3)'_{\text{s}}$		1176.5	6.2	
$\nu(\text{C}-\text{O}) \text{ s}$		1034.2	98.1	1033.1, 1030.6
$\nu(\text{C}-\text{O}) \text{ as}$		1004.6	348.5	1002.3, 998.7
$\nu(\text{S}-\text{O}) \text{ as}$		807.8	234.2	837.5, 834.5, 830.6
$\nu(\text{S}-\text{O}) \text{ s}$		743.1	101.3	771.0
$\gamma(\text{SO}_2)$		580.6	14.1	590.9
$w(\text{SO}_2)$		537.3	15.9	553.6
$\delta(\text{O}=\text{S}=\text{O})$		504.7	14.8	523.2, 521.3
$\text{tw}(\text{SO}_2)$		403.9	13.4	420.7, 417.1
$\delta(\text{OSO})$		390.7	5.4	402.7

B3LYP/aug-cc-pVQZ calculated frequencies and intensities are given for comparison. Frequencies in  $\text{cm}^{-1}$ ; s calculated intensities in  $\text{km mol}^{-1}$ ;  $\nu$ : bond stretching;  $\delta$ : bending;  $\gamma$ : rocking,  $\tau$ : torsion;  $w$ : wagging;  $\text{tw}$ : twisting; s: symmetric; as: asymmetric. See Table S02 for definition of symmetry coordinates.

<sup>a</sup> Frequencies in bold correspond to bands due to the conformer embedded in its most stable sites in the matrix (see text). Additional experimental bands due to overtones and combination tones involving the  $\delta\text{CH}_3$  bending modes are observed at 2921.9, 2900.0, 2865.5, 2847.1 and 2842.6  $\text{cm}^{-1}$ . Besides, a band due the  $[\nu(\text{C}-\text{O}) \text{ as} + \text{tw}(\text{SO}_2)]$  combination mode is observed at 1434.1  $\text{cm}^{-1}$ . The relatively broad bands observed at 1410.7, 1409.3, 1402.8, 1400.2  $\text{cm}^{-1}$  are ascribable to the  $\nu(\text{S}=\text{O})$  mode in small size aggregates present in the matrices in low concentration.

<sup>b</sup> An additional band due the  $[\nu(\text{C}-\text{O}) \text{ as} + \text{tw}(\text{SO}_2)]$  combination mode is observed at 1431.8  $\text{cm}^{-1}$ .

next section, the experimental observations fully confirm the theoretical predictions presented above.

### 3.2. Vibrational spectra

Dimethyl sulfate has 33 fundamental vibrations. For both GG ( $C_2$ ) and GT ( $C_1$ ) conformers, all fundamental vibrations are active in the infrared. Table S02 (ESI) displays the definition of symmetry coordinates used in the normal coordinates analysis undertaken in this study. The B3LYP/aug-cc-pVQZ calculated spectra for all the conformers of DMSO<sub>4</sub> (including the TT form) and potential energy distributions (PEDs) are given in Tables S03–S05 (ESI). Vibrational assignments for the spectra of the compound isolated in argon matrices are displayed in Table 2.

Fig. 3 shows the spectrum of DMSO<sub>4</sub> freshly deposited in an argon matrix at 9 K, using the temperature of sublimation of 298 K. The calculated spectra for conformers GG and GT are also displayed for comparison, fitting nicely the experimental data. As pointed out above, in the gaseous phase, at 298 K, conformer GG is the most populated form (its estimated population is nearly twice that of GT) and, as expected, the bands due to this species dominate the spectra of the matrix-isolated compound.

The single previously reported study of the vibrational spectra (both infrared and Raman) of DMSO<sub>4</sub> in the liquid phase [9] assumed, on the basis of the measured depolarization ratios of the observed Raman bands, a  $C_{2v}$  geometry for the molecule, corresponding to the planar TT form. As shown in the previous section, the TT conformer (which in-

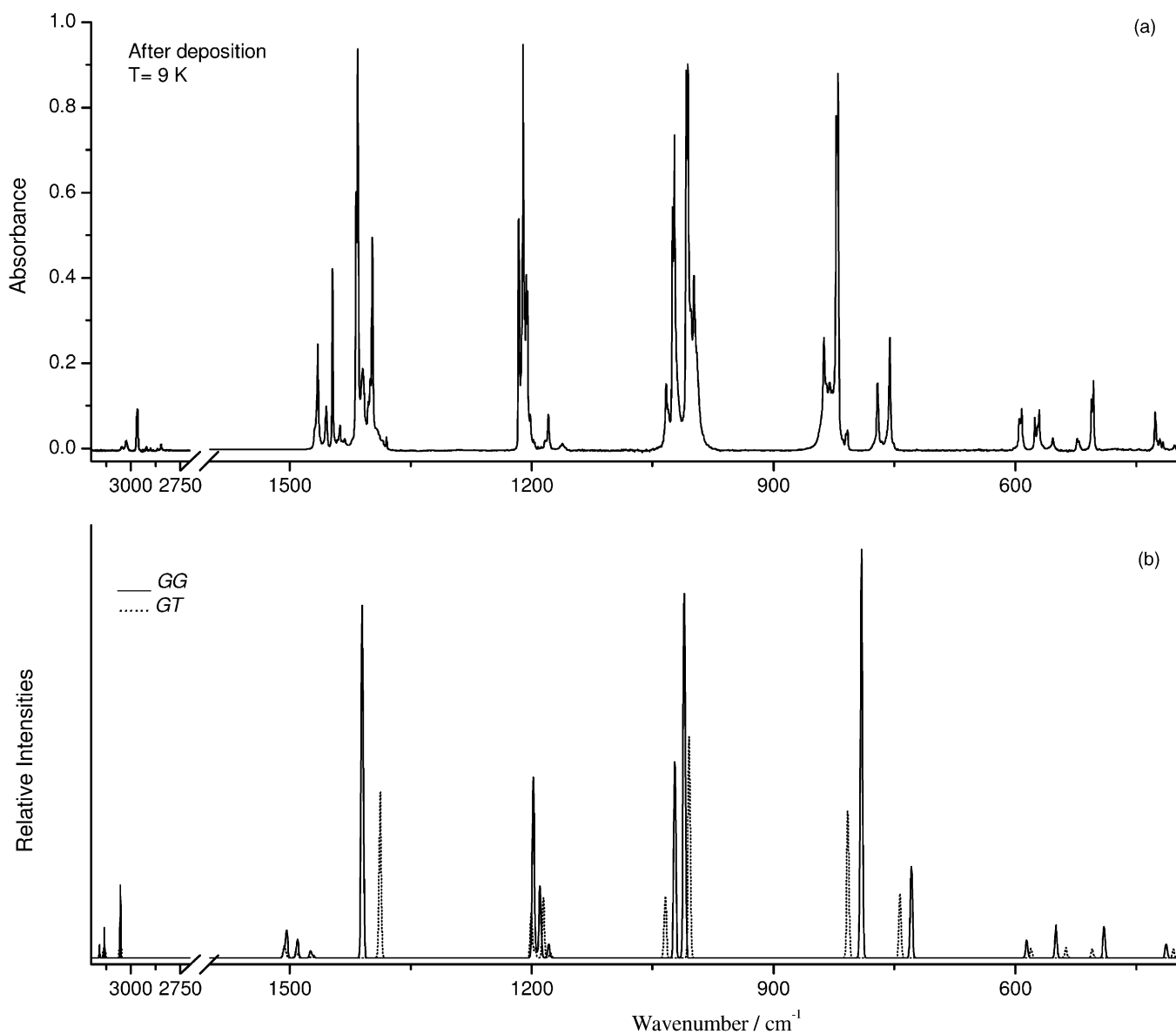


Fig. 3. Infrared spectra of DMSO<sub>4</sub>: (a) isolated in an argon matrix ( $T=9$  K); (b) B3LYP/aug-cc-pVQZ calculated spectra for GG and GT conformers (weighted by the B3LYP/aug-cc-pVQZ estimated populations at 298 K (see Table 1).

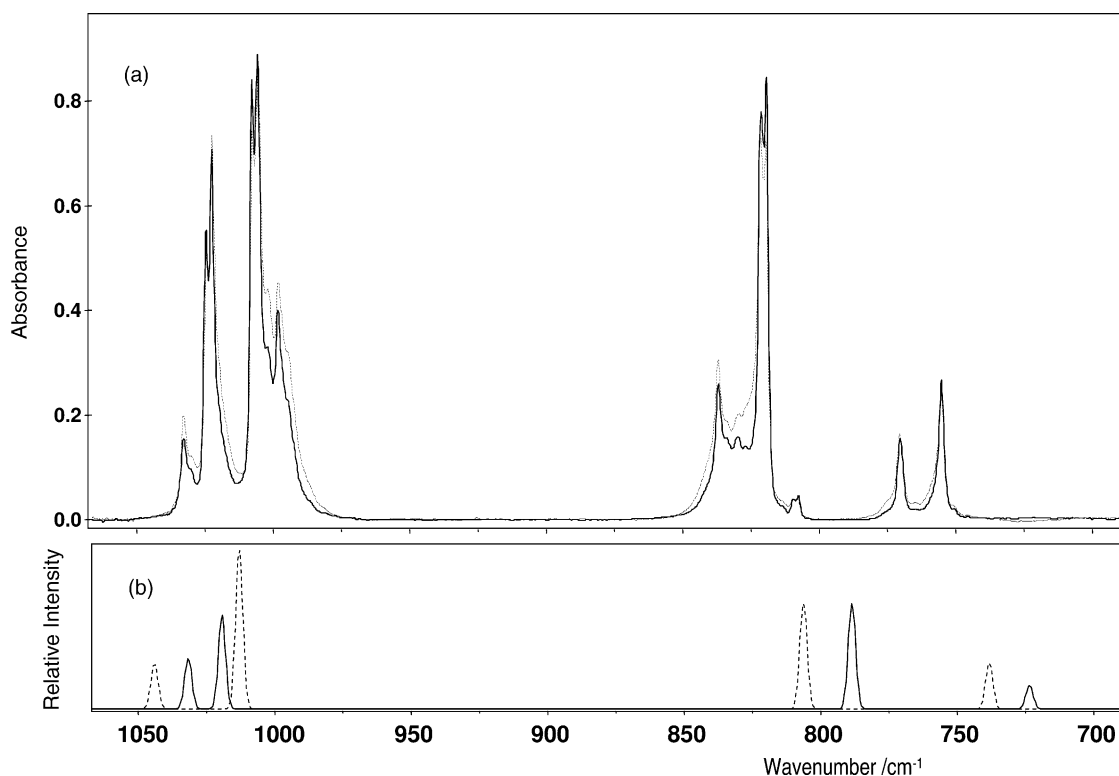


Fig. 4. (a) Spectral region ( $1050\text{--}700\text{ cm}^{-1}$ ) of the infrared spectra of  $\text{DMSO}_4$  trapped in an argon matrix obtained immediately after deposition at 9 K using nozzle temperatures of 298 K (solid line) and 463 K (dashed line); (b) B3LYP/aug-cc-pVQZ-calculated spectra for GG (solid line) and GT conformers (dashed line) [weighted by the B3LYP/aug-cc-pVQZ estimated populations at 298 K (see Table 1)].

deed is now predicted to have a slightly non-planar skeleton, thus belonging to the  $C_2$  point group) does not correspond to an observable species. Its stabilization in the liquid phase is not expected as well, since its dipole moment is smaller than those of the GG and GT conformers. Besides, in the previous study of  $\text{DMSO}_4$  [9], the possible existence of more than one conformational state was ignored. Hence, reinterpretation of the spectra of liquid  $\text{DMSO}_4$ , on the light of the present study shall deserve further attention.

The general assignment of the spectra could be easily undertaken by comparing the calculated and experimental results obtained in the present study, as well as the previous data obtained for the pure liquid [9]. However, the precise identification of the bands due to each conformer required, besides that information, both the comparison of spectra obtained using different nozzle temperatures (Fig. 4) and interpretation of the matrix annealing experiments (Fig. 5). In the first type of experiments, increasing of the nozzle temperature leads to increase the population of the less stable GT conformer in the gas phase, immediately prior to deposition. Accordingly, bands due to this conformer increase relatively to those originated in the most stable GG form. Fig. 4 shows the  $1050$  and  $700\text{ cm}^{-1}$  spectral region of the spectra obtained immediately after deposition of the matrices using the nozzle temperatures of 298 and 463 K, and compares the experimental spectra with the theoretical predictions (B3LYP/aug-cc-pVQZ calculated spectra for GG and GT

forms, weighted by their estimated relative populations at 298 K). Note that besides the relative increase of intensity of the bands due to GT, the spectrum of the sample deposited using the higher nozzle temperature does also exhibit some evidence of presence of a small amount of aggregates in the matrix (e.g., shoulders appearing in the high frequency wings of the bands in the  $850\text{--}750\text{ cm}^{-1}$  region as well as in the low frequency wings of the bands in the  $1050\text{--}950\text{ cm}^{-1}$  region), which are a consequence of local heating due to the arrival of the hot gaseous beam. Using the calculated relative intensities as weighting factors, the relative energy of the two experimentally observed conformers could be estimated from the integral intensities of bands ascribed to the individual conformers. The averaged value, estimated using the experimental data obtained for the four nozzle temperatures used (298, 393, 423 and 463 K), was  $5 \pm 1\text{ kJ mol}^{-1}$ , is in good agreement with the relative energies predicted by the highest level calculations (B3LYP/aug-cc-pVQZ:  $3.71\text{ kJ mol}^{-1}$ ; MP2/6-31++G(d,p):  $5.41\text{ kJ mol}^{-1}$ ; see Table 1).

Also in consonance with the theoretical predictions, upon annealing of the matrix, bands due to GT decrease intensity while those ascribed to GG increase, indicating conversion from the higher energy conformer to the most stable form (see Fig. 5). Very interestingly, the GG form was found to occupy two distinct substitutional matrix sites, one of them being considerably more stable than the other.

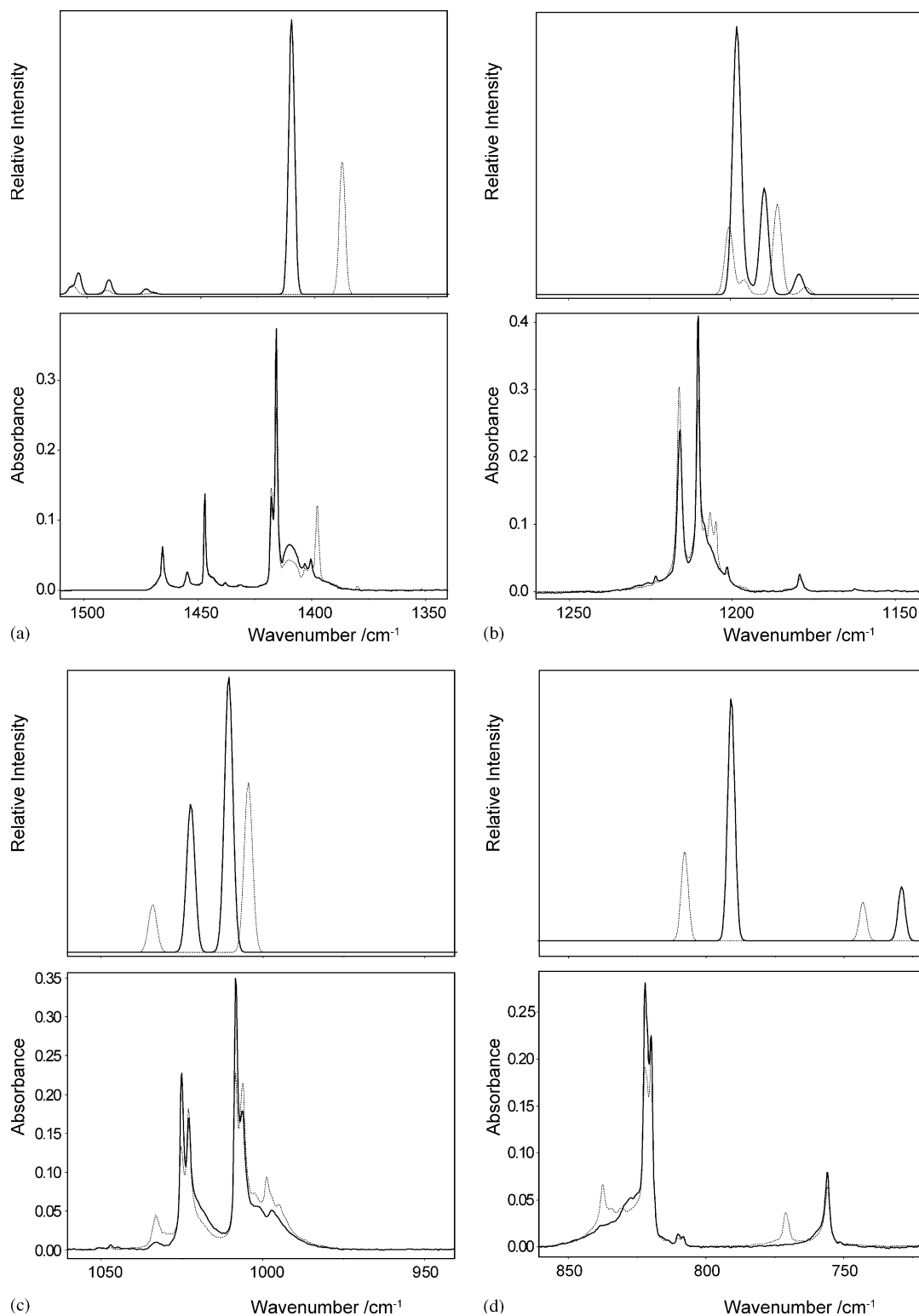


Fig. 5. Infrared spectra of DMSO<sub>4</sub> trapped in an argon matrix obtained immediately after deposition at 9 K (dashed line) and after annealing at 25 K (solid line) and calculated spectra for GG (solid line) and GT (dashed line) conformers [weighted by the B3LYP/aug-cc-pVQZ estimated populations at 298 K (see Table 1)]: (a) 1500–1350 cm<sup>-1</sup> region; (b) 1250–1150 cm<sup>-1</sup> region; (c) 1050–950 cm<sup>-1</sup> region; (d) 850–700 cm<sup>-1</sup> region; (e) 600–450 cm<sup>-1</sup> region. Top spectra are calculated; bottom spectra are obtained experimentally.

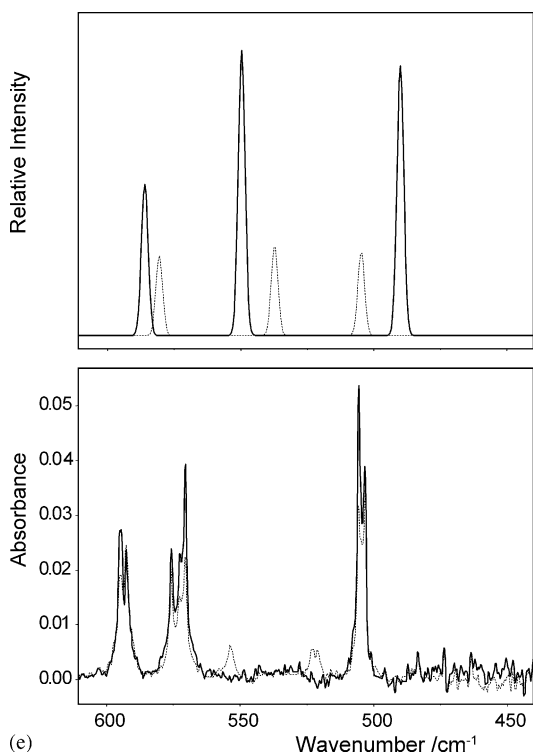


Fig. 5. (Continued.)

Indeed, at 41 K, the spectrum is dominated by bands due to aggregates, the only bands due to monomeric forms still remaining observable being those originated in form GG in the most stable site (Fig. 6). At 25 K, most of the GT conformer was already converted into GG, and the results show that GT gives rise to GG in its most stable site, whereas at this temperature the intensity of the bands due to molecules of GG occupying its less stable site were found to decrease very slightly relatively to that observed in the as-deposited matrix. The small reduction of intensity observed in the bands due to GG in the less stable site indicates that site relaxation is also occurring in a small extension. Above 25 K, the bands ascribed to the less stable GG site decrease faster, while those assigned to the most stable GG site also start to decrease, in consequence of aggregation. The greater facility of the less stable GG site molecules to aggregate as compared with those occupying the most stable site is clearly revealed by the experimental data (see Fig. 6), and is also consistent with the relative stability of the two local environments.

In summary, the matrix-isolation experiments fully confirm the theoretical predictions regarding the type and relative stability of the two observable conformers of DMSO<sub>4</sub>. Conformer GG is the most stable conformer in both the gaseous phase and isolated in argon, occupying to different substitutional sites in the matrix with different

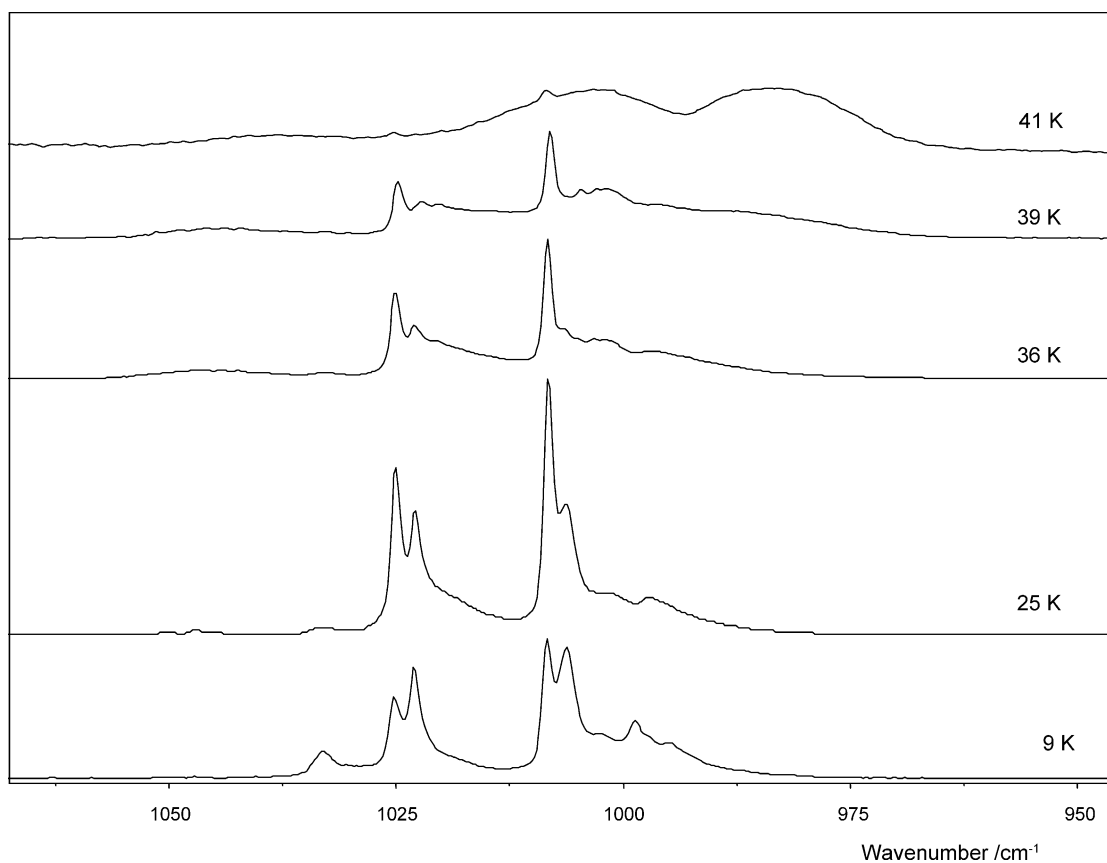


Fig. 6. Infrared spectra of DMSO<sub>4</sub> trapped in an argon matrix (1050–950 cm<sup>-1</sup> region). Results of high temperature annealing showing changes due to conversion of conformer GT into GG (in the first stages of annealing) and of molecular aggregation.

stabilities. Upon annealing of the matrix, the less stable conformer (GT) quickly converts to the GG conformer, with the resulting species being embedded in a site which corresponds to the most stable matrix-site for GG form. Further annealing leads to extensive aggregation; however, even at 41 K, where the aggregates strongly dominate, some amount of GG monomer occupying its most stable site can still be observed experimentally. Also in agreement with the theoretical predictions, the highest energy TT conformer was not observed in the spectra of the matrix-isolated compound.

#### 4. Conclusion

The preferred conformations of dimethyl sulfate and their vibrational spectra were investigated by a concerted approach based on the matrix-isolation method coupled with FT-IR spectroscopy and theoretical methods. Conformer GG was found to be the most stable conformer of the compound in both the gaseous phase and isolated in argon. In the matrices, this form was shown to exist in two different matrix cages, with different stabilities. Upon annealing of the matrix, conformer GT quickly converts to the GG conformer, the resulting species being embedded in its most stable possible matrix cage. The vibrational spectra of the two observed conformers were fully assigned on the basis of temperature variation studies (both annealing and variation of the nozzle temperature experiments were undertaken) and theoretical predictions of their infrared spectra. The highest energy TT conformer, which was assumed previously to be the most stable conformer [9], is predicted by the calculations to have a relative energy of ca.  $10 \text{ kJ mol}^{-1}$  and was not observed in the spectra of the matrix-isolated compound.

#### Acknowledgements

This work was supported by the Portuguese *Fundação para a Ciência e a Tecnologia* (Research Project POCTI/QUI/43366/2001 and Grant FCT SFRH/BPD/11499/2002), FEDER, CONICET, and Agencia Nacional de Promoción Científica y Tecnológica-PICT 13080, Argentina.

#### Appendix A. Supplementary data

Supplementary data associated with this article can be found, in the online version, at [doi:10.1016/j.saa.2004.10.050](https://doi.org/10.1016/j.saa.2004.10.050).

#### References

[1] Du Pont, Dimethyl Sulfate Properties, Uses, Storage and Handling, E.I. Du Pont de Nemours & Co. Inc, Wilmington, Delaware, 1981, pp.24.

[2] National Institute for Occupational Safety and Health (NIOSH), Information Profiles on Potential Occupational Hazards. I. Single Chemicals I. Dimethyl Sulfate, NIOSH, Rockville, MD, 1979, pp. 9.

[3] A. Dzhazhev, D. Tsvetkov, *Gig. i Sanit* 35 (1970) 7 (in Russian).

[4] L. Fishbein, US Environmental Protection Agency Bulletin, Washington, DC, 1977, p. 319.

[5] L. Alvarez, M. Hurtt, G. Kenned, *Drug Chem. Toxicol.* 20 (1997) 99.

[6] B. Mathison, M. Taylor, M. Bogdanffy, *Fund. Appl. Toxicol.* 28 (1995) 255.

[7] WHO, World Health Organization Bulletin, WHO, Geneva, 1986.

[8] I.A. Zheltukhin, N.I. Glybochko, A.S. Sobolev, T.S. Maslakova, *Anal. Abstr.* 46 (1984) 941.

[9] K.O. Christe, E.C. Curtis, *Spectrochim. Acta A* 28 (1972) 1889.

[10] A.H. Zeng, L. Yu, Y. Wang, Q.Y. Kong, Q. Xu, M.F. Zhou, *J. Phys. Chem. A* 108 (2004) 6656.

[11] U.S. Department of Health and Human Services, Azardous Substances Data Bank (HSDB, online database), U.S. National Library of Medicine, U.S. National Toxicology Information Program, Bethesda, MD, 1993.

[12] R. Ray, B.J. Benton, D.R. Anderson, S.L. Byers, J.P. Petrali, *J. Appl. Toxicol.* 20 (2000) S87.

[13] J.P. Petrali, S. Oglesby-Megee, *Microsc. Res. Technol.* 37 (1997) 221.

[14] I. Reva, S. Stepanian, L. Adamowicz, R. Fausto, *J. Phys. Chem. A* 105 (2001) 4773.

[15] M.J. Frisch, G.W. Trucks, H.B. Schlegel, G.E. Scuseria, M.A. Robb, J.R. Cheeseman, V.G. Zakrzewski, J.A. Montgomery Jr., R.E. Stratmann, J.C. Burant, S. Dapprich, J.M. Millam, A.D. Daniels, K.N. Kudin, M.C. Strain, O. Farkas, J. Tomasi, V. Barone, M. Cossi, R. Cammi, B. Mennucci, C. Pomelli, C. Adamo, S. Clifford, J. Ochterski, G.A. Petersson, P.Y. Ayala, Q. Cui, K. Morokuma, D.K. Malick, A.D. Rabuck, K. Raghavachari, J.B. Foresman, J. Cioslowski, J.V. Ortiz, A.G. Baboul, B.B. Stefanov, G. Liu, A. Liashenko, P. Piskorz, I. Komaromi, R. Gomperts, R.L. Martin, D.J. Fox, T. Keith, M.A. Al-Laham, C.Y. Peng, A. Nanayakkara, C. Gonzalez, M. Challacombe, P.M.W. Gill, B. Johnson, W. Chen, M.W. Wong, J.L. Andres, C. Gonzalez, M. Head-Gordon, E.S. Replogle, J.A. Pople, Gaussian '98, Revision A. 9, Gaussian Inc., Pittsburgh, PA, 1998.

[16] A.D. McLean, G.S. Chandler, *J. Chem. Phys.* 72 (1980) 5639.

[17] R. Krishnan, J.S. Binkley, R. Seeger, J.A. Pople, *J. Chem. Phys.* 72 (1980) 650.

[18] R. Ditchfield, W.J. Hehre, J.A. Pople, *J. Chem. Phys.* 54 (1971) 724.

[19] W.J. Hehre, R. Ditchfield, J.A. Pople, *J. Chem. Phys.* 56 (1972) 2257.

[20] T.H. Dunning Jr., *J. Chem. Phys.* 90 (1989) 1007.

[21] T. Clark, J. Chandrasekhar, G.W. Spitznagel, P.v.R. Schleyer, *J. Comp. Chem.* 4 (1983) 294.

[22] D.E. Woon, T.H. Dunning Jr., *J. Chem. Phys.* 98 (1993) 1358.

[23] R.A. Kendall, T.H. Dunning Jr., R.J. Harrison, *J. Chem. Phys.* 96 (1992) 6796.

[24] C. Moller, M.S. Plesset, *Phys. Rev.* 46 (1934) 618.

[25] M. Frisch, M. Head-Gordon, J.A. Pople, *Chem. Phys. Lett.* 166 (1990) 281.

[26] A. Becke, *Phys. Rev. A* 38 (1988) 3098.

[27] C. Lee, W. Yang, R. Parr, *Phys. Rev. B* 37 (1988) 785.

[28] P. Csaszar, P. Pulay, *Theochemistry* 114 (1984) 31.

[29] C. Peng, H.B. Schlegel, *Isr. J. Chem.* 33 (1994) 449.

[30] J. Schachtschneider, Technical Report, Shell Development Co., Emeryville, CA, 1969.

[31] A. Givan, L.A. Larsen, A. Loewenschuss, C.J. Nielsen, *J. Mol. Struct.* 509 (1999) 35.